SAE INTERNATIONAL®

Applying Complex Turbulent Cross-Correlation Function to an SEA Side Glass to Predict Interior Wind Noise

2016-01-1830
Published 06/15/2016

Denis Blanchet
ESI

Luca Alimonti
ESI US R&D

Anton Golota
ESI

CITATION: Blanchet, D., Alimonti, L., and Golota, A., "Applying Complex Turbulent Cross-Correlation Function to an SEA Side Glass to Predict Interior Wind Noise," SAE Technical Paper 2016-01-1830, 2016, doi:10.4271/2016-01-1830.

Abstract

This paper presents new advances in predicting wind noise contribution to interior SPL in the framework of the Wind Noise German Working Group composed of Audi, Daimler, Porsche and VW. In particular, a new approach was developed that allows to fully describe the wind noise source using CFD generated surface pressure distribution and its cross-correlation function and apply this source on an SEA side glass. This new method removes the need to use a diffuse acoustic field or several plane waves with various incidence angle to approximate the correct acoustics source character to apply on the SEA side glass. This new approach results are compared with results previously published which use more deterministic methods to represent the side glass and the interior of a vehicle.

Introduction

Several methods of representing the wind noise sources have been investigated over the past 10 years in the automotive industry. Empirical methods have shown their merits and limitations especially when the geometry of the structure changes significantly compared to previous computations [1,2,3,4]. A more predictive approach, based on the ability of coupling time domain turbulent flow data to a vibro-acoustics model has opened new possibilities.

This paper introduces the current windnoise modeling methods used and previously published before showing where this new cross-correlation approach fits in the computation process. Then a review of the validation of the current approach is done. It describes the experimental setup in the wind tunnel, the CFD data and a description of the three vibro-acoustics models (BEM, FE-SEA Coupled, SEA) used in comparison between experimental results and the simulation results. And last, the theory of the new cross-correlation approach is introduced. Various analysis are performed to assess the accuracy of the new approach and finally this approach is compared with previously published results for comparison.

Current windnoise modeling method

This section is aimed at familiarizing the reader to previous work that has been published in the last 2 years [5]. Figure 1 summarize the computation process investigated. The left side of Figure 1 shows the source characterization approach available and the right side the vibro-acoustics methods that can be combined to compute the interior SPL. In this work, the combination of an aero-acoustic (CAA) source model with a vibro-acoustic (VA) model is called an aero-vibro-acoustic (AVA) model. Figure 1 shows the process for three different computations. All computations in this study are based on CFD compressible data unless otherwise stated. See “CFD data” section for more details.

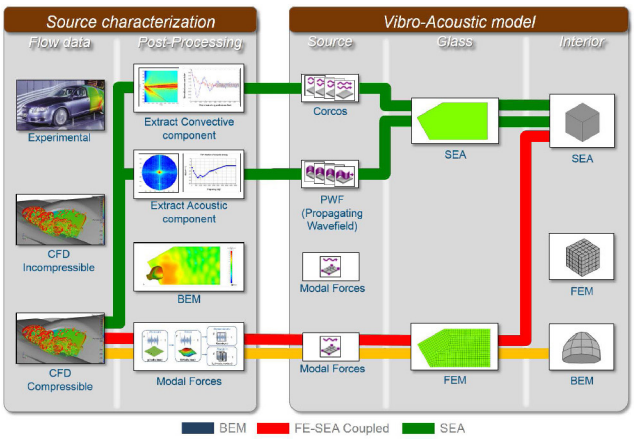

Figure 1. Illustration of source characterization (left) and vibro-acoustic modelling (right) approaches discussed in this paper. Three cases are studied: BEM, FE-SEA Coupled and SEA

For the "BEM" and "FE-SEA Coupled" cases, modal forces are used to represent the turbulent flow and a FEM side glass is used in conjunction with a BEM or SEA interior fluid. This approach has the advantage of being accurate, provided that the source data is accurate, since the time domain CFD source data is taken as is, converted into modal forces, applied on a FEM panel. In the case of the BEM results, a deterministic BEM interior fluid is used. This approach is highly accurate and is computationally intensive. Model setup can generally be achieved within a day or two. In the case of the "FE-SEA Coupled" case, a SEA interior fluid cavity is used to increase frequency range of computation to higher frequencies than the glass coincidence. It is also used to reduce computation time since only a few degrees of freedom is needed to represent the interior fluid. The model setup is simple and can be completed in a few hours.

For the SEA case, the convective component is extracted from the data to find the Corcos parameters to be use with this empirical turbulent flow model. The acoustic component is evaluated using the 2D wavenumber transform described in [5]. A SEA side glass is used in conjunction with a SEA interior fluid. The SEA side glass is excited with the corcos source and several acoustic planes waves with various angle of incidence onto the side glass to approximate the acoustic waves travelling from the mirror and the A and B pillars toward the side glass. This approach has the advantage of being fast to compute. Once both components of turbulent flow are extracted, the wind noise contribution to interior SPL is computed in minutes.

Turbulent Cross-Correlation Function on SEA panel

The subject of this paper is to introduce the newly implemented user-defined cross-correlation source which can be assigned to a SEA panel. This new source has the advantage of retaining the complexity of the turbulent flow cross-correlation character to apply onto a SEA panel. As will be demonstrated later in this study, this approach is more precise than using a set of plane waves traveling towards the side glass with various headings. Figure 2 shows where this new post-processing of flow data and vibro-acoustic source fits into the existing realm of possible approaches.

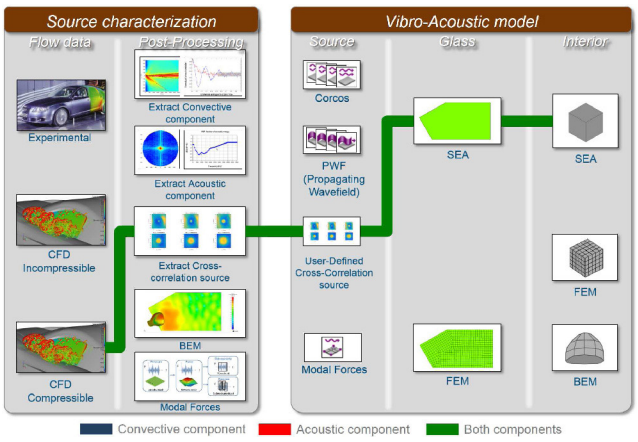

Figure 2. Full AVA process from source to receiver for the case when a user-defined cross correlation source is used

Note that this new post-processing method can be used to extract the convective and acoustic component separately allowing the user to assess the contribution of both components to the vehicle interior noise separately. This will be the object of a future publication.

Validation of Current Aero-Vibro-Acoustic Models

Experimental Setup

The measurements are described in details in [6]. Figure 3 shows on the left the SAE body in the wind tunnel for the configuration where the vibrations on side glass and SPL inside the SAE body are measured. The right side of the figure shows the surface mounted microphones used to measure the fluctuating surface pressure at the location of the side glass.

Figure 3. Wind-tunnel test: (a) glass module, (b) sensor module

Figure 4 shows in more details the microphones used to measure the fluctuating surface pressure.

Figure 4. Surface microphones over side glass area.

CFD data

The CFD data used for the prediction of wind noise inside the SAE body was computed by the German Working Group. See [6] for details:

- StarCCM+ Version 6.06.017
- Half model of an SAE body, a very basic car shape on struts, with a rear mirror
- Model size: ~45 million fluid cells
- Compressible Detached Eddy Simulation (DES) based on Spalart-Allmaras (S-A)
- Δt CFD = 2E-05s
- First 0.1s of simulated physical time has been cut away: spurious transition phenomena when starting a transient computation based on steady state results

The pressure time history data was imported into the commercial vibro-acoustics software in [7].

Aero-Vibro-Acoustic (AVA) models

Figure 5 shows the SEA model containing a SEA side glass structural panel, an area junction and a SEA interior fluid. The sources representing the turbulent flow fluctuating pressures are divided into

a convective component (Corcos) and an acoustic component (PWF). Source levels and parameters were extracted from the CFD data based on earlier sections. This model runs in seconds.

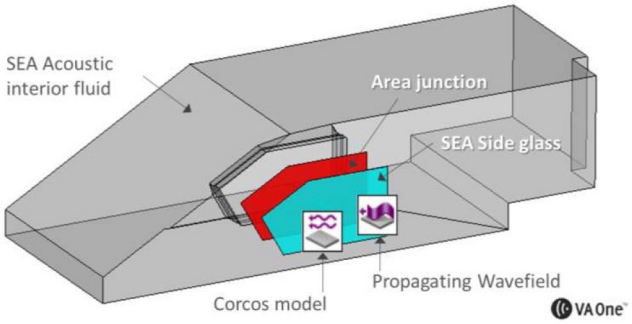

Figure 5. SEA model including SEA interior fluid, SEA side glass panel, area junction and wind noise sources.

Figure 6 shows the FE/SEA Coupled model containing a FEM side glass structural panel, an area junction and a SEA interior fluid. The FE/SEA method has been widely used in various industries over the past 10 years. An introduction to FE/SEA Coupled can be found in [8] and detailed theory in [9,10]. The source representing the turbulent flow is a time domain Fluctuating Surface Pressure (FSP) where the time domain CFD data is converted into frequency domain modal forces as described in an earlier section.

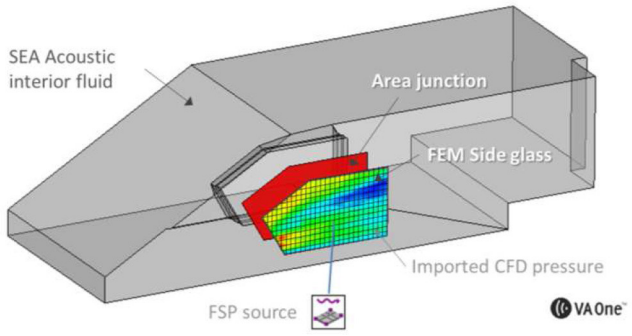

Figure 6. FE/SEA Coupled model including interior SEA fluid, FEM side glass panel, area junction and time domain wind noise source.

Figure 7 shows the BEM model. For clarity, a mesh with coarse element size was used to generate the image but of course a smaller element size is needed to compute to higher frequencies.

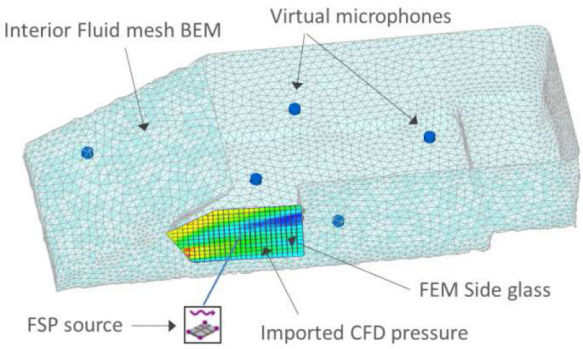

Figure 7. BEM model including FEM side glass, BEM interior fluid and a wind noise (FSP) source.

The mesh size for both the BEM fluid and the structural FEM panel follows the 6 elements per wavelength criteria. The BEM mesh allows for the prediction of SPL at any location inside and outside the SAE body. Five virtual microphones were located at the same location as in the measurements. A time domain FSP (Fluctuating Surface Pressure) source is connected to the side glass to allow the CFD data to be read in the model and converted into frequency domain modal forces as described in an earlier section. Imported CFD pressure data can be visualized as a contour plot in the current frequency domain set in the BEM model as shown in figure 7.

AVA Validation Results

The following results are only presented as illustration of correlation accuracy that has been achieved so far on a few configurations. It does not constitute a recommendation of preferred approaches but the status of the current study and merely an indication of what are the next results that will be published at a later time.

Figure 8 shows the average SPL inside the SAE body generated by a 140 km/h wind and the presence of a side mirror predicted using the SEA model. The average SPL is a combination of the convective and acoustic component where the convective contributes at lower frequency and the acoustic at higher frequency. Results are presented in 1/12th octave. One can note that at higher frequencies, the response from a single Propagating Wave Field (PWF) underpredicts the response. Previous experience has shown that using a Diffuse Acoustic Fields (DAF) overpredicts the response and clearly do not properly represent the acoustic component's wave propagation since it assumes that waves have the same probability of hitting the side glass from any angles. The use of 5 PWF on the side glass already improves the correlation with measurements. Further studies are underway to understand how to best model the acoustic component.

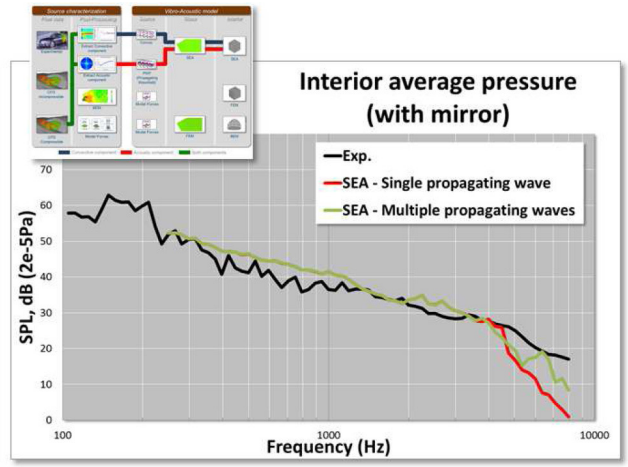

Figure 8. Average SPL inside SAE body generated by 140 km/h wind predicted using a SEA model.

Figure 9 shows the average SPL inside SAE body generated by a 140 km/h wind and the presence of a side mirror predicted using the FE/SEA Coupled model.

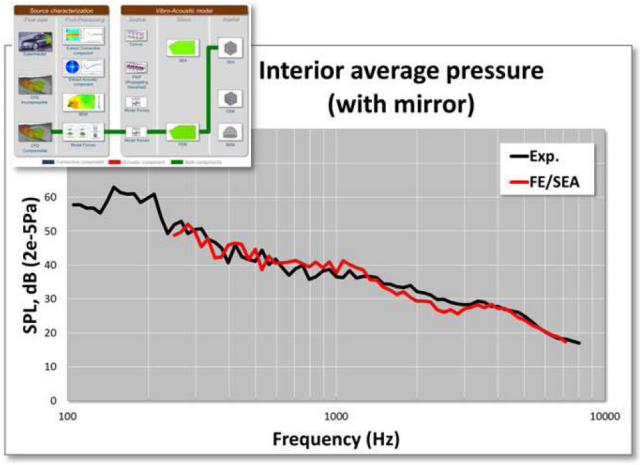

Figure 9. Average SPL inside SAE body generated by 140 km/h wind predicted using a FE/SEA Coupled model.

The modal forces approach was used. The level of correlation between the measurement and the predicted level is very high. This modelling approach offers a nice alternative to SEA since accuracy is higher and only the side glass has to be modelled in FEM. The use of modal forces provides a better representation of the excitation over the whole side glass area. Computation time is of course large than with SEA since the time domain CFD data has to be processed and the modal basis of the side glass computed and used in the coupled computation. Figure 10 shows the correlation between measurements and the BEM model in 1/12th octave. The modal forces approach was used. The correlation level is higher than the two previous approaches thanks to the BEM representation of the interior fluid.

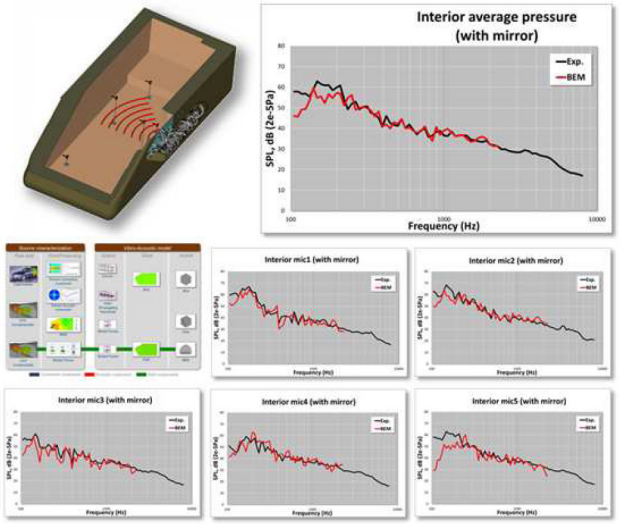

Figure 10. Average and single microphone SPL inside SAE body generated by 140 km/h wind predicted using a BEM model.

The BEM approach can also compute SPL at specific microphone locations. Note that each microphone shows the same level of correlation as the average does. This further confirms that the CFD results and the VA model are quite accurate since the AVA model yield such a level of correlation. All BEM computation are shown until a little over 2000 Hz due to the computational expense.

It is also interesting to look at the same data in different frequency ranges. Figure 11 shows the data in 1/3rd octave bands and 10Hz constant bandwidth. The 1/3rd octave band results show a difference of only a few dBs at frequencies higher than 300 Hz. The 10 Hz bandwidth shows the character of the response in more details.

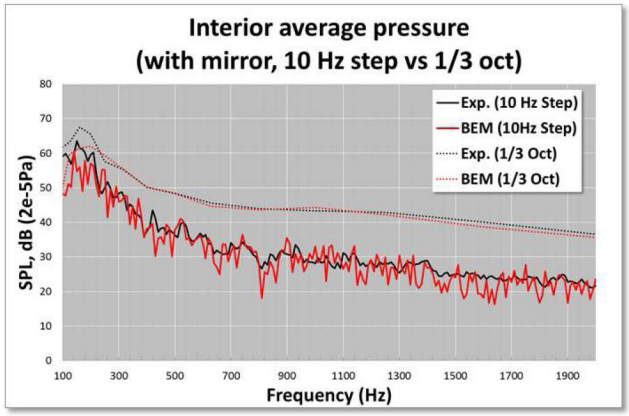

Figure 11. Average SPL inside SAE body generated by 140 km/h wind predicted using a BEM model in 1/3rd octave and 10 Hz frequency step resolution

It can be seen that the predicted response has a more peaky character. This is explained by the fact that the measurements were averaged over a period of 30 seconds as opposed to the CFD data which was computed for less than 0.5 seconds. One should also note that the conversion of the time signal into frequency domain was done in a deterministic way; the time signal was not averaged and no overlapping windows were used, the whole time period available was directly converted into the frequency domain.

New Cross-Correlation Source Applied to SEA

This section describes the new complex cross-correlation source that can be applied on a SEA panel.

Theory

The response of a dynamic system excited by a random excitation is of interest. We assume the excitation to be a stationary and homogeneous random process, i.e. the statistics up to second order are independent of the observation point in space and time (wide-sense stationary). Such excitation is a random pressure fluctuation that directly drives a structure (i.e. the side glass). The latter is backed by an acoustic fluid (i.e. the interior cabin). The system is assumed flat and the average power injected into the structural system and transmitted to the fluid domain are of interest.

Consider a generic flat plate excited by a random pressure load $p(x,t)$, on one side and radiating in an acoustic medium on the other side. Following [11,12], the total power injected into the plate flexural wavefield in a given frequency band can be formally written as

$$\Pi_{\text{in}}(\omega_c) = \frac{1}{\pi}\int_{\omega_1}^{\omega_2}\int_{\mathbf{x}} \text{Re}\{S_{pv}(\mathbf{x},\omega)\}\text{d}\mathbf{x}\,\text{d}\omega = \frac{1}{\pi}\int_{\omega_1}^{\omega_2} S_{\Pi_{\text{in}}}(\omega)\,\text{d}\omega \quad (1)$$

where S_{pv} is the cross-correlation (one-sided space-frequency spectrum) between the external load p and the the structural velocity v (i.e. time derivative of the plate out of plane displacement). The spectrum $S_{\Pi_{in}}$ is thus the spectral density of the power injected into the plate. The considered frequency band is characterized by a center circular frequency ω_c with upper and lower bounds ω_1 and ω_2, respectively. Similarly, the spectral density of the power radiated into the acoustic medium is

$$\Pi_{\mathrm{rad}}(\omega_c) = \frac{1}{\pi}\int_{\omega_1}^{\omega_2}\int_{\mathbf{x}} \mathrm{Re}\{S_{p_a v}(\mathbf{x},\omega)\}\mathrm{d}\mathbf{x}\,\mathrm{d}\omega = \frac{1}{\pi}\int_{\omega_1}^{\omega_2} S_{\Pi_{\mathrm{rad}}}(\omega)\,\mathrm{d}\omega \tag{2}$$

where p_a is the acoustic pressure in the fluid medium at the interface with the structure. Using the definition of the cross-correlation and invoking the Parseval theorem to move from the physical space **x** to the wavenumber space **k**, one can express the spectral densities $S_{\Pi_{in}}$ and $S_{\Pi_{rad}}$ as integrals in the wavenumber space. In the context of the wave approach to SEA, one obtains,

$$S_{\Pi_{\mathrm{in}}}(\omega) = S_{pp_0}(\omega)\frac{A}{4\pi^2}\int_{\mathbf{k}} \mathrm{Re}\{Y_{\sim}(\mathbf{k},\omega)\}\,\Gamma_{pp}(\mathbf{k},\omega)\}\,\mathrm{d}\mathbf{k} \tag{3}$$

for the power input, and

$$S_{\Pi_{\mathrm{rad}}}(\omega) = S_{pp_0}(\omega)\frac{A}{4\pi^2}\int_{\mathbf{k}<\bar{\mathbf{k}}} \mathrm{Re}\{z_{\infty}(|\mathbf{k}|,\omega)\}\,|Y_{\sim}(\mathbf{k},\omega)|^2\,\Gamma_{pp}(\mathbf{k},\omega)\,\mathrm{d}\mathbf{k} \tag{4}$$

for the power non resonantly radiated into the cavity. The spectral density of the pressure load is S_{pp_0}. The area of the plate is A. The mobility of the infinite plate is $Y_{\sim}(\mathbf{k}, \omega)$, while $\Gamma_{pp}(\mathbf{k}, \omega)$, is the normalized wavenumber frequency spectrum of the source. The plane wave radiation impedance of the receiver fluid is referred to as $z_{\infty}(|\mathbf{k}|, \omega)$. Note that the integral involved in Eq. (4) is limited to the wavenumber space confined to the area shared between the mass-law controlled region of the plate mobility and the acoustic circle (i.e. only non-resonant transmission is accounted for).

In the context of a modal approach to SEA, one can instead write,

$$S_{\Pi_{\mathrm{in}}}(\omega) = S_{pp_0}(\omega)\,A^2 \sum_{\omega_{mn}\in\Delta\omega} \mathrm{Re}\{Y_{mn}(\omega)\}\,J^2_{mn}(\omega) \tag{5}$$

and

$$S_{\Pi_{\mathrm{rad}}}(\omega) = S_{pp_0}(\omega)\frac{\rho_0\omega k_0}{2\pi}A^4 \sum_{\omega_{mn}<\omega_1} |Y_{mn}(\omega)|^2\,J^2_{mn,\infty}(\omega)\,J^2_{mn}(\omega) \tag{6}$$

for the spectral density of the power injected into the plate and non resonantly transmitted to the cavity.
$Y_{mn}(\omega) = i\omega\,N_{mn}/M_{mn}(\omega^2_{mn} - \omega^2)$ is the modal mobility operator, with modal normalization factor N_{mn} and modal mass M_{mn}. The density of the fluid is ρ_0 and the acoustic wavenumber is k_0. The summation in Eq. (5) extends to the modes that resonate in the considered frequency band $\Delta\omega$, whereas that in Eq. (6) is limited to the mass-controlled modes (i.e. with natural frequency smaller than the lower limit of the band). The above equations require the computation of the modal joint acceptances J^2_{mn} and $J^2_{mn,\infty}$. These are defined as

$$J^2_{mn}(\omega) = \frac{1}{A^2}\frac{1}{4\pi^2}\int_{\mathbf{k}} |\phi_{mn}(\mathbf{k})|^2\Gamma_{pp}(\mathbf{k},\omega)\,\mathrm{d}\mathbf{k} \tag{7}$$

$$J^2_{mn,\infty}(\omega) = \frac{2\pi}{k_0 A^2}\frac{1}{4\pi^2}\int_{\mathbf{k}} \frac{|\phi_{mn}(\mathbf{k})|^2}{k_0\sqrt{1-(|\mathbf{k}|/k_0)^2}}\,\mathrm{d}\mathbf{k} \tag{8}$$

which are a measure of how well a given mode shape (ϕ_mn) couples with the external load and the receiving fluid, respectively.

Hence, both modal and wave based powers require the computation of 2-D integrals in the wavenumber domain involving the wavenumber-frequency spectrum of the fluctuating pressure load $\Gamma_{pp}(\mathbf{k}, \omega)$. The latter is computed by Fourier transforming the CFD data. In the present work, the periodogram estimate is employed to obtain the wavenumber spectrum from the spatial FFT of the time-space pressure signal (Refs. [6,7]).

External Fluctuating Pressure

The fluctuating surface pressure varies significantly over the surface of a side glass. Patches have been used to study the character of the turbulence in various region of the glass (Figure 12).

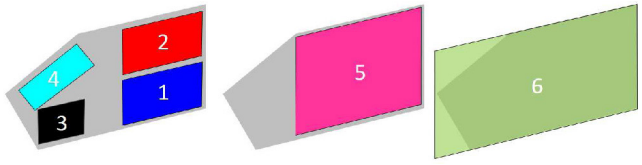

Figure 12. Left: Patch 1 & 2 in reattached area, patch 3 in mirror wake and patch 4 in APillar vortex. Center: Large inscribed patch. Right: Circumscribed patch

Figure 13 shows the external fluctuating pressure spectra of the various patches. The raw CFD data (approx. 1mm mesh size) is used on patches 1 to 4. The same data is also mapped onto a 5mm FE mesh for the patch 5 and a 5 and 10mm FE mesh for the patch 6.

The choice of the patch size affects the resolution in the wavenumber domain and, consequently, the accuracy of SEA analysis. A small patch allows for a fast computation of the wavenumber spectrum but it is likely to give a poor resolution in the wavenumber space, which

potentially jeopardizes the accuracy of the acoustic component. On the other hand, a large patch increases the spectral resolution at the cost of intensifying the computational burden and memory usage. Moreover, the use of a large patch that can cover most of the excited surface is preferable as it gives a better estimate of the average load (this aspect may be important for highly non homogeneous loads). For these reasons, it is interesting to assess the possibility of mapping the original CFD data on a coarser mesh in order to reduce the computational effort. The target mesh is supposed to adequately represent the bending wavenumber of the plate up to the maximum frequency of analysis. Therefore, the mapped pressure fluctuation will involve less nodes compared to the original CFD data set (e.g. 1mm to 5mm and 10 mm mesh in the considered examples), making it possible to reduce the computational burden when a large patch is used. Note that a suitable mapping scheme was used to avoid aliasing effects in mapping from the fine (CFD) the coarse mesh.

It should be noted that, for complex planar geometries, it may be difficult to perfectly fit a large patch to the loaded surface. If the patch is larger than the glass (e.g. patch 6), pressure data is not available everywhere over the patch, so that the computed wavenumber spectrum may contain artifacts. On the other hand, a smaller patch could avoid such source of error but will not be able to cover the whole loaded surface, thus possibly leading to a less accurate estimate of the average load.

Figure 13 quantifies the degree of non homogeneity of the considered source. The average surface pressure of patches 3-4 is 10 dB above the surface pressure of patches 1-2. Furthermore, the surface pressure of the patch 5 shows lower pressure levels than patch 6 since the highly energetic region around patches 3 and 4 is omitted from the analysis. Also, a “patch 1 incompressible” (computed separately) is compared with “patch 1” and shows similar results. This is expected since the hydrodynamic component of the side glass turbulence dominates the exterior surface pressure spectrum, the acoustic component can be 30 to 70 dB smaller in amplitude than the convective component. Despite this fact, the acoustic component contributes significantly to the vehicle interior noise because it couples more efficiently with the side glass than the convective component. The reference curve on all graphs is a BEM computation based on the work done in section “AVA validation results”.

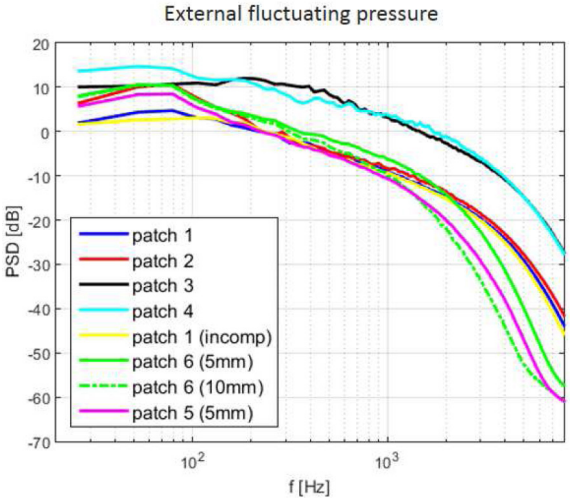

Figure 13. External fluctuating pressure spectra for various patches

Effect on Plate and Cavity Energy

Figure 14 and 15 compares the energy levels of the side glass and the interior cavity. The wave approach is used to compute the SEA input powers (See Theory section)) and CLF. It shows that for patch 1 and above 300 Hz, the system is mainly driven by the acoustic loading. This is easily observed by comparing the “patch 1” with the “patch 1 incompressible” curves. Another interesting observation is that even though there is a 10 dB difference in the external fluctuating pressure between patch 1-2 and patch 3-4, the energy levels are relatively similar for all patches close to coincidence frequency at around 3500 Hz. Finally, results confirm goodness of the mapping procedure since the 10mm mesh size results match the 5mm mesh size results, meaning that the filtered wavenumbers do not drive the structure (i.e. the hydrodynamic component is "too short" to inject power into the structure).

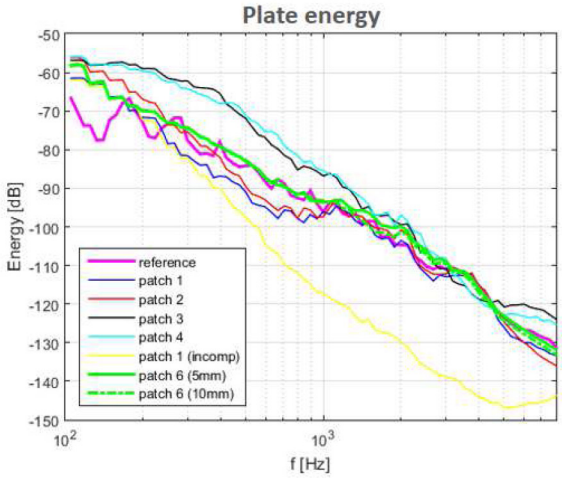

Figure 14. Plate energy for various patches

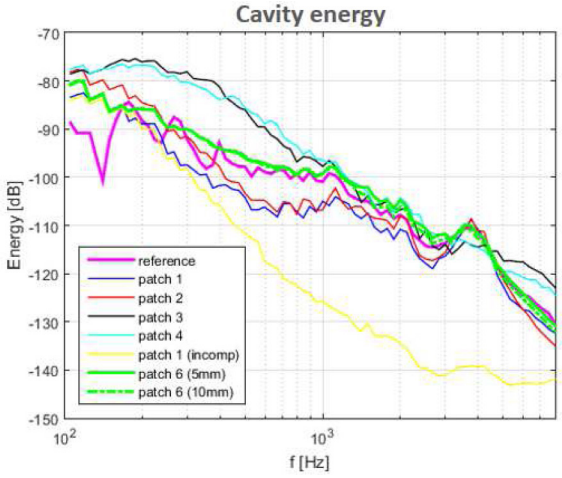

Figure 15. Cavity energy for various patches

In the coming section, the selection of the proper analysis region on the side glass is discussed. Factors to consider are region size, mesh density, CPU time and memory/storage usage.

Patch 6 vs Small Patches Average

Figure 16 compares the effect of choosing patch 6 compared to an arithmetic average of the patches 1 to 4. As can be seen, the average of the small patches does not properly represent the physics at low frequency where the hydrodynamic component dominates. Patches 3-4 are not large enough to accurately represent the acoustic

component of the wavenumber spectrum in the low frequency range, due to the lack of resolution. This probably pollutes the average. At frequencies between 1000 and 5000Hz, the response is driven by the acoustic component which seems to be well represented using a simple average of the small patches. Over 5000 Hz, results diverge and this approach is not accurate.

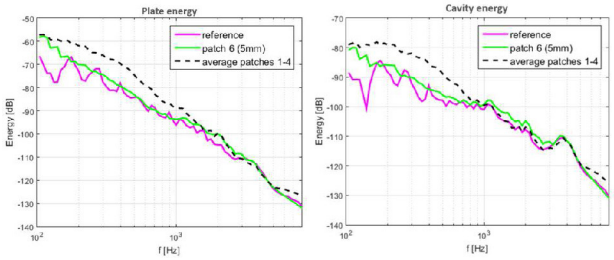

Figure 16. Comparison of plate and cavity energy for patch 6 vs small patches average

Patch 5 Considerations

Figure 17 shows the importance of accounting for the portion of glass behind the mirror wake and the APillar vortex (patches 3 and 4). The latter is excluded patch 5, so the response is underestimated (follows patches 1-2 only).

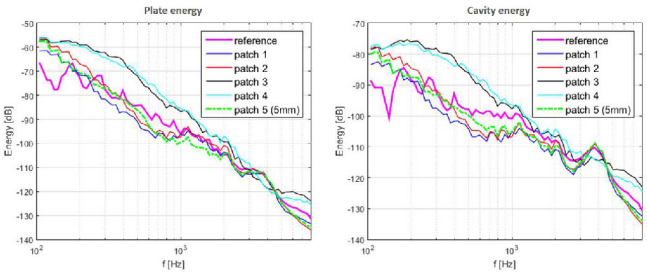

Figure 17. Comparison of plate and cavity energy for patch 5 vs small patches and reference case

Weighted Average

Fig 18 suggests that a weighted average using patches 3,4 and 5 may be an effective strategy to increase the accuracy of the prediction. This is confirmed in fig 17. Results are promising and improve correlation overall and especially above 5000 Hz.

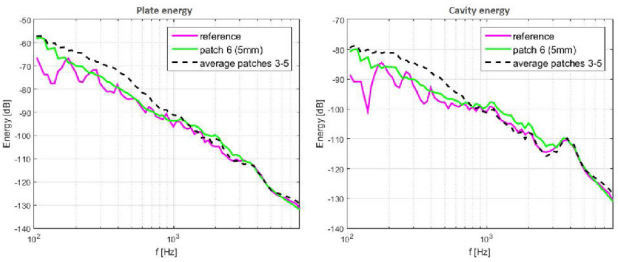

Figure 18. Comparison of plate and cavity energy for patch 6 vs area weighted average of patches 3 to 5

Wave vs Modal CLF Computation

In figure 19, the results obtained by means of the wave approach are compared with a modal based SEA model. Results refer to patch 6. It can be observed that the two methodologies give consistent results, despite the low modal density of the side glass which prevents from having enough modes in the low frequency range (i.e. below 1 KHz). It should be also noted that the difference between wave and modal approach observed around the coincidence frequency (4 KHz) is due to the approximation used to compute the CLF in the modal approach (see [7]).

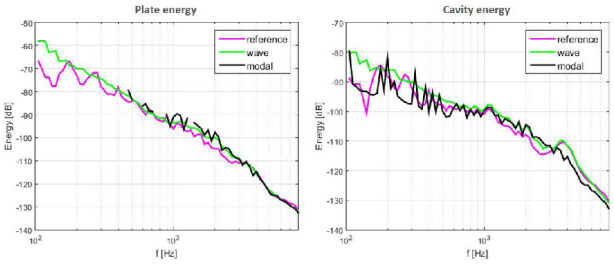

Figure 19. Comparison of plate and cavity energy for patch 6 using modal or wave formulation for CLF computation between glass and interior cavity

Final Results

The work in previous sections leads to the conclusion that the best compromise to predict wind noise contribution to SPL inside a vehicle using SEA and the user-defined cross-correlation function described in this paper is to use the patch 6 results since they are the ones that best fit the reference case on the full frequency spectrum. Even though this case present drawbacks since generally, a rectangular box larger than the side window should be avoided as it results in discontinuities of the pressure being FFTed. This generates noise along the direction of the discontinuities. An area weighted average is proposed to avoid such source of error. Indeed, the area weighted average greatly improves the accuracy in the region between 1 and 3 KHz, where the lack of pressure data in patch 6 is likely to generate artificial size effects (thus overestimating the response).

In a design process, when looking for the most efficient process to compute accurate interior noise levels, one can imagine using BEM up to 1000 Hz and use SEA with this new user-defined cross-correlation source to compute the response at higher frequencies using the weighted patch approach since it provides essentially identical results as the highly computationally demanding BEM method in this frequency range.

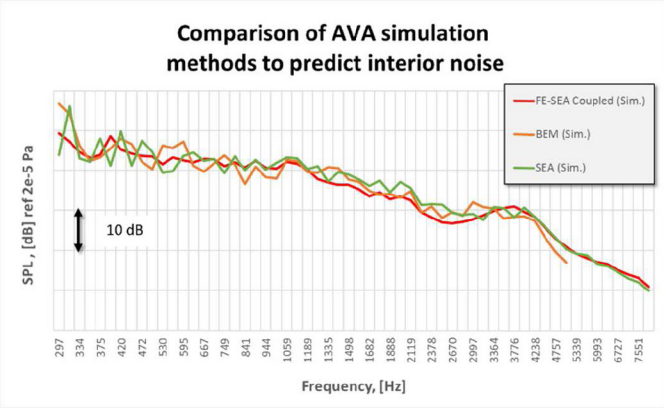

Figure 20. Comparison of AVA simulation methods to predict vehicle interior noise

Figure 20 shows the correlation between various simulation methods using the same CFD data as input. The SEA curve corresponds to the patch 6 case and compares favorably with the “FE-SEA Coupled”

and the BEM case confirming that the user-defined cross-correlation approach provides accurate representation of wind noise source and that used in conjunction with a purely SEA model, one can accurately predicts wind noise contribution to vehicle interior noise levels.

Conclusions

This paper has demonstrated that the new user-defined cross-correlation source implementation can be used to accurately represent turbulent surface pressure such as wind excitation on a side glass. It has also demonstrated that a simple SEA model can be used with this new user-defined source to accurately predict the contribution of windnoise to a vehicle interior noise level. Finally, it has been shown that the use of a circumscribed patch is today's best compromise to get accurate prediction of interior noise on a full frequency range and that an area weighted average approach is more accurate in the frequency range higher than 1000 Hz.

References

1. DeJong, R., Bharj, T., and Lee, J., "Vehicle Wind Noise Analysis Using a SEA Model with Measured Source Levels," SAE Technical Paper 2001-01-1629, 2001, doi:10.4271/2001-01-1629.
2. DeJong, R., Bharj, T., and Booz, G., "Validation of SEA Wind Noise Model for a Design Change," SAE Technical Paper 2003-01-1552, 2003, doi:10.4271/2003-01-1552.
3. Peng, G., "SEA Modeling of Vehicle Wind Noise and Load Case Representation," SAE Technical Paper 2007-01-2304, 2007, doi:10.4271/2007-01-2304.
4. Kralicek, J., Blanchet, D., "Windnoise: Coupling Wind Tunnel Test Data or CFD Simulation to Full Vehicle Vibro-Acoustic Models", DAGA, Düsseldorf, Germany, 2011,
5. Blanchet, D. and Golota, A., "Combining Modeling Methods to Accurately Predict Wind Noise Contribution," SAE Technical Paper 2015-01-2326, 2015, doi:10.4271/2015-01-2326.
6. Hartmann, M., Ocker, J., Lemke, T., Mutzke, A. et al., "Wind Noise caused by the A-pillar and the Side Mirror flow of a Generic Vehicle Model", 18th AIAA/CEAS Aeroacoustics Conference, Paper 2012-2205, Colorado Springs, USA, 2012.
7. VA One 2016, The ESI Group. http://www.esi-group.com
8. Blanchet, D.: "FE/SEA Coupled", 10 years after first implementation, Aachen Acoustic Colloquium, Aachen, Germany, 2014,
9. Shorter, P.J. and Langley, R.S.: Vibro-acoustic analysis of complex systems, Journal of Sound and Vibration, 2004,
10. Shorter, P.J., and Langley, R.S., "On the reciprocity relationship between direct field radiation and diffuse reverberant loading". JASA,117, 85-95, 2005,
11. Maury, C., Gardonio, P. and Elliott, S.J. "A wavenumber approach to modelling the response of a randomly excited panel, part i: General theory". Journal of Sound and Vibration, 252(1):83 - 113, 2002.
12. Maury, C., Gardonio, P. and Elliott, S.J. " A wavenumber approach to modelling the response of a randomly excited panel, part ii: Application to aircraft panels excited by a turbulent boundary layer". Journal of Sound and Vibration, 252(1):115 - 139, 2002.

Contact Information

Luca.Alimonti@esi-group.com

Acknowledgments

The authors would like to thank the CAA German Working Group composed of Audi, Daimler, Porsche and VW for authorizing ESI to use their experimental and CFD data for the VA and AVA validation work presented in this study.

Definitions/Abbreviations

SEA - Statistical Energy Analysis

BEM - Boundary Element Method

FSP - Fluctuating Surface Pressure: Time domain source type in VA One

TBL - Turbulent Boundary Layer: Corcos model of turbulent flow: Frequency domain source in VA One

PWF - Propagating wavefield: Waves impinging on a panel at a specific angle: Frequency domain source in VA One

FEM - Finite Element Method

DAF - Diffuse Acoustic Field: Random incidence wave field: Frequency domain source in VA One

SPL - Sound pressure level

Corcos - Empirical model describing a complex turbulent flow

FE/SEA Coupled - Method that fully couples FEM and SEA in a unique vibro-acoustic model

VA - Vibro-Acoustics

AVA - Aero-vibro-Acoustics

SAE - Society of Automotive Engineers

SAE body - Generic automobile shape

CFD - Computational Fluid Dynamics

DES - Detached Eddies Simulation

CAA - Computational Aeroacoustics

CLF - Coupling Loss Factor

The Engineering Meetings Board has approved this paper for publication. It has successfully completed SAE's peer review process under the supervision of the session organizer. The process requires a minimum of three (3) reviews by industry experts.

ISSN 0148-7191

http://papers.sae.org/2016-01-1830